© 2017. Published by The Company of Biologists Ltd | Journal of Cell Science (2017) 130, 1475-1485 doi:10.1242/jcs.198937

RESEARCH ARTICLE

Missing-in-metastasis protein downregulates CXCR4 by promoting ubiquitylation and interaction with small Rab GTPases

Lushen Li[1,2], Shaneen S. Baxter[2], Ning Gu[1], Min Ji[1] and Xi Zhan[2,3,4,*]

ABSTRACT

Surface expression of chemokine receptor CXCR4 is downregulated by missing-in-metastasis protein (MIM; also known as MTSS1), a member of the inverse BAR (I-BAR)-domain protein family that recognizes and generates membranes with negative curvature. Yet, the mechanism for the regulation is unknown. Here, we show that MIM forms a complex with CXCR4 by binding to E3 ubiquitin ligase AIP4 (also known as ITCH) in response to stromal cell-derived factor 1 (SDF-1; also known as CXCL12). Overexpression of MIM promoted CXCR4 ubiquitylation, inhibited cellular response to SDF-1, caused accumulation and aggregation of multivesicular bodies (MVBs) in the cytoplasm, and promoted CXCR4 sorting into MVBs in a manner depending on binding to AIP4. In response to SDF-1, MIM also bound transiently to the small GTPase Rab5 at 5 min and to Rab7 at 30 min. Binding to Rab7 requires an N-terminal coiled-coil motif, deletion of which abolished MIM-mediated MVB formation and CXCR4 internalization. Our results unveil a previously unknown property of MIM that establishes the linkage of protein ubiquitylation with Rab-guided trafficking of CXCR4 in endocytic vesicles.

KEY WORDS: MIM, CXCR4, Ubiquitylation, AIP4, Rab7, MVBs

INTRODUCTION

Chemokine receptor CXCR4 plays an important role in the interaction of hematopoietic stem cells with bone marrow (BM) niches and is often downregulated through internalization after exposure to its ligand stromal cell-derived factor 1 (SDF-1; also known as CXCL12) (Marchese, 2014). The intracellular process of CXCR4 internalization is initiated upon phosphorylation at its C-terminus, followed by ubiquitylation and subsequent sorting into early endosomes, which are then processed into late endosomes or multivesicular bodies (MVBs) and further fused with lysosomes, in which the receptor and its bound ligand are degraded. The maturation of endosomes involves a cascade of cellular processes that is controlled by Rab small GTPases (Guerra and Bucci, 2016; Mizuno-Yamasaki et al., 2012). In particular, the transition from Rab5 to Rab7 enrichment on membranes signals the maturation of MVBs, which contain characteristic intraluminal vesicles. Yet the molecular mechanism responsible for such a transition has not been defined.

MIM, or metastasis suppressor 1 (MTSS1), gene was identified as a putative metastasis suppressor (Lee et al., 2002; Nixdorf et al., 2004) that is aberrantly expressed in many advanced cancers (Agarwal et al., 2017; Liu et al., 2010; Mertz et al., 2014; Parr and Jiang, 2009; Schemionek et al., 2015a,b; Xie et al., 2011; Yu et al., 2012) and may play a complicated role under different pathological contexts. The N-terminal motif of MIM protein is homologous to a Bin-Amphiphysin-Rvs (BAR) domain, which is present in many proteins that are involved in membrane dynamics by binding to specific phospholipid membranes through a curved interface (Zimmerberg and McLaughlin, 2004). While most BAR domains have a positively charged concave surface, the BAR domain of MIM displays an inverse, or convex exterior (Lee et al., 2007; Saarikangas et al., 2009), and is able to promote filopodia-like protrusive extensions (Saarikangas et al., 2009). This feature is also found in four other mammalian proteins, which together with MIM make up the I-BAR protein subfamily. Disruption of the MIM gene in mice generates several abnormalities, including kidney dysfunction (Saarikangas et al., 2011; Xia et al., 2010), neuronal dendritic spines (Saarikangas et al., 2015) and the tendency to develop B cell malignancies in aged mice (Yu et al., 2012). We have recently reported that bone marrow (BM) cells derived from a MIM knockout (KO) mouse strain exhibit impaired internalization of CXCR4 and enhance CXCR4-mediated homing of stem cells to the BM and CXCR4 signaling in response to its primary ligand SDF-1 (Zhan et al., 2016). Identification of the function of MIM in CXCR4 internalization is consistent with the phenotype of the aged MIM KO mice that tend to develop B cell malignancies (Yu et al., 2012) as CXCR4 plays a critical role in the interaction of hematopoietic stem cells with their niches, and aberrant CXCR4 activation or internalization has been implicated in B cell malignancies (McCormick et al., 2009; Spiegel et al., 2004). However, our current understanding of the function of MIM provides little information about its role in the regulation of receptor-mediated endocytosis. Although a few BAR domain-containing proteins have been implicated in the establishment of clathrin-coated pits, during which they remodel the plasma membrane into a topology with positive curvature (Daumke et al., 2014; Dawson et al., 2006), MIM generates membranes with a negative curvature, the role of which in the endocytic pathway remains undefined. In the presented study, we attempted to investigate the mechanism by which MIM regulates CXCR4 internalization. We found that MIM is a multifunctional protein that is associated with endocytic vesicles. Instead of just being a simple membrane remodeling protein, it promotes receptor ubiquitylation after SDF-1 stimulation, transiently binds to Rab5 and Rab7 at times corresponding to the transition from early endosomes to late endosomes, and promotes MVB biogenesis and CXCR4 trafficking into MVBs. Hence, MIM uses a newly identified cellular mechanism for ligand-directed endocytosis by acting as an effector of Rab GTPases as well as an activator for protein ubiquitylation.

[1]School of Biological Science and Medical Engineering, Southeast University, Nanjing 210096, China. [2]Center for Vascular and Inflammatory Diseases, University of Maryland School of Medicine, Baltimore, MD 21201, USA. [3]Department of Pathology, University of Maryland School of Medicine, Baltimore, MD 21201, USA. [4]University of Maryland Marlene and Stewart Greenebaum Comprehensive Cancer Center, Baltimore, MD 21201, USA.

*Author for correspondence (xzhan@som.umaryland.edu)

N.G., 0000-0003-0047-337X; X.Z., 0000-0003-3291-3050

Received 25 October 2016; Accepted 27 February 2017

Journal of Cell Science

Journal of Cell Science (2017) 130, 1475-1485 doi:10.1242/jcs.198937

RESULTS

Overexpression of MIM promotes CXCR4 internalization

To verify the role of MIM in the regulation of CXCR4, we transfected a plasmid encoding MIM–GFP into HeLa cells, which otherwise poorly express endogenous MIM (Fig. S1E). Unlike cells expressing GFP only, which strongly responded to SDF-1 by undergoing chemotaxis in a dose-dependent manner, the cells stably expressing MIM–GFP showed only weak responses to SDF-1 (Fig. 1A,B). Flow cytometry revealed that the surface of MIM–GFP cells had 20% CXCR4 remaining after exposure to SDF-1 for 15 min, whereas the surface of control cells, which expressed GFP only, had more than 60% CXCR4 remaining under the same condition (Fig. 1C-E), indicating that forced MIM expression promoted CXCR4 internalization. We also examined several CXCR4 downstream signaling factors, including MAP kinases MAPK3 and MAPK1 (also known as ERK1 and ERK2; Erk1/2) (Fig. 1F) and p38 proteins (the antibody used here recognizes MAPK14, -11 and -12) (Fig. 1G), and small GTPases Rac1 (Fig. 1H) and Cdc42 (Fig. 1I). Except for Erk1/2, which was phosphorylated to a greater extent in MIM–GFP cells than in control cells, activation of p38 proteins, Rac1 and Cdc42 was less prominent in MIM–GFP cells. Although increased Erk1/2 phosphorylation is commonly implicated in cell proliferation, MIM–GFP cells did not show significant growth advantage over control cells (data not shown). Overall, MIM–GFP-expressing HeLa cells responded to SDF-1 in a manner opposite to that of bone marrow cells derived from MIM KO mice (Zhan et al., 2016). Hence, MIM–GFP HeLa cells were used as a model to investigate the role of MIM in the regulation of cellular responses to CXCR4.

MIM promotes CXCR4 ubiquitylation

We first examined the effect of MIM on CXCR4 degradation following exposure to SDF-1, one of the events that occurs after internalization (Marchese and Benovic, 2001). In the absence of protein synthesis, CXCR4 had a half-life of about 8 h in bone marrow cells derived from MIM KO mice (Fig. 2A) or about 7 h in GFP cells (Fig. 2B) after exposure to SDF-1. Conversely, CXCR4 had a half-life of about 3 h in bone marrow cells from WT mice (Fig. 2A) or MIM–GFP-expressing cells (Fig. 2B). Next, we investigated whether MIM promotes CXCR4 degradation through ubiquitylation (Marchese et al., 2003). GFP- and MIM–GFP-expressing cells were co-transfected with Myc-tagged CXCR4 (Myc–CXCR4) and hemagglutinin (HA)-tagged ubiquitin (HA–Ub), and the co-transfectants were exposed to SDF-1 for 30 min. Ubiquitylated Myc–CXCR4 in the treated cells was estimated by immunoprecipitation (IP) using either an antibody against Myc followed by western blotting for HA (Fig. 2C) or vice versa (Fig. 2D). Both approaches demonstrated that SDF-1 triggered stronger Myc–CXCR4 ubiquitylation in MIM–GFP cells than that in GFP cells.

MIM promotes the interaction between AIP4 and CXCR4 in response to SDF-1

CXCR4 ubiquitylation is known to be catalyzed by E3 ubiquitin ligase AIP4 (also known as ITCH) (Marchese, 2009). Therefore, we examined the effect of MIM on the interaction between Flag–AIP4 and Myc–CXCR4 co-expressed in GFP or MIM–GFP cells. Although a small (Myc–CXCR4)–(Flag–AIP4) interaction in GFP cells was detected upon SDF-1 treatment, such interaction was markedly enhanced in MIM–GFP cells (Fig. 2E). We also examined endogenous CXCR4 and AIP4 in mouse-derived cells and observed that the interaction between them was severely impaired in bone marrow cells derived from MIM KO mice (Fig. 2F). Hence, MIM-mediated CXCR4 degradation was correlated with its potential to facilitate AIP4 to target CXCR4.

MIM forms a complex with CXCR4 via binding to AIP4

IP analysis using an antibody against either Myc or GFP further demonstrated that MIM–GFP consistently formed a complex with Myc–CXCR4 (Fig. 3A,B) and Flag–AIP4 (Fig. 3C) upon SDF-1 treatment. Interactions among these proteins were also examined by confocal microscopy, which revealed that both MIM–GFP and Flag–AIP4 proteins were expressed in a diffuse and punctate manner in the cytoplasm (Fig. 3D). In untreated cells, MIM–GFP colocalized poorly with Flag–AIP4. Yet, their colocalization was more apparent in SDF-1-treated cells. Quantitative analysis of the digital images based on Manders' overlapping coefficient (MOC) showed that nearly 60% of Flag–AIP4 was colocalized with MIM–GFP in SDF-1-treated cells, which is ∼fivefold of that in untreated cells. Similar analysis also demonstrated that about 60% of Myc–CXCR4 localized with MIM–GFP in the SDF-1-treated cells, which is also ∼fivefold of that in untreated cells (Fig. 3E).

In an effort to define the molecular mechanism by which MIM interacts with AIP4, we first examined the serine-rich domain (SRD), which corresponds to the region from amino acids 242 to 363, and a proline-rich domain (PRD) near the C-terminus (Fig. 4A) because AIP4 contains four WW domains, which recognize either PRDs (Chen and Sudol, 1995) or phosphorylated serine or threonine residues preceding a proline residue (Lu et al., 1999). Deletion of the PRD abolished the interaction with AIP4 in response to SDF-1 (Fig. 4B), whereas deletion of the SRD did not have any impact on the interaction (Fig. 4B). Further mutagenesis revealed that deletion of a PPLP motif, one of the preferred targets of AIP4 (Bedford et al., 1997) and located within the PRD, severely impaired AIP4 binding (Fig. 4C).

CXCR4 does not contain an apparent motif for targeting MIM protein. Thus, we speculated that MIM might bind to CXCR4 indirectly through AIP4. Indeed, MIMΔPRD–GFP, which was unable to bind to AIP4, was also unable to interact with Myc–CXCR4 (Fig. 4D). In contrast, the mutant MIMΔSRD–GFP bound to CXCR4 as effectively as MIM–GFP (Fig. 4D). To confirm the role of AIP4 in the interaction of MIM with CXCR4, expression of endogenous AIP4 in cells expressing MIM–GFP and Myc–CXCR4 was suppressed by transfecting a mixture of siRNAs against AIP4. These siRNAs inhibited AIP4 expression by more than 80% and effectively abolished the SDF-1-mediated interaction between MIM–GFP and Myc–CXCR4 (Fig. 4E). To further determine the role of binding to AIP4 in the MIM-mediated cellular response to SDF-1, cells expressing MIMΔPRD–GFP were analyzed. Unlike MIM–GFP, overexpression of MIMΔPRD–GFP failed to induce a significant increase of Myc–CXCR4 ubiquitylation (Fig. 4F), to suppress SDF-1-mediated chemotaxis (Fig. 4G) and to promote CXCR4 internalization (Fig. 4H). Hence, MIM facilitates CXCR4 internalization via the function of AIP4.

MIM promotes sorting of CXCR4 into MVBs

The above data implied that MIM has a function in endocytic vesicles. This assumption is supported by the prompt colocalization of nearly 50% EE1A, a marker of early endosomes, with MIM–GFP at 5 min after SDF-1 treatment (Fig. S1A). By the same time, ∼60% of EE1A colocalized with Myc–CXCR4 (Fig. S1B) and over 60% of Myc–CXCR4 colocalized with MIM–GFP (Fig. S1C). Remarkably, at 30 min, MIM–GFP-expressing cells displayed a

Journal of Cell Science (2017) 130, 1475-1485 doi:10.1242/jcs.198937

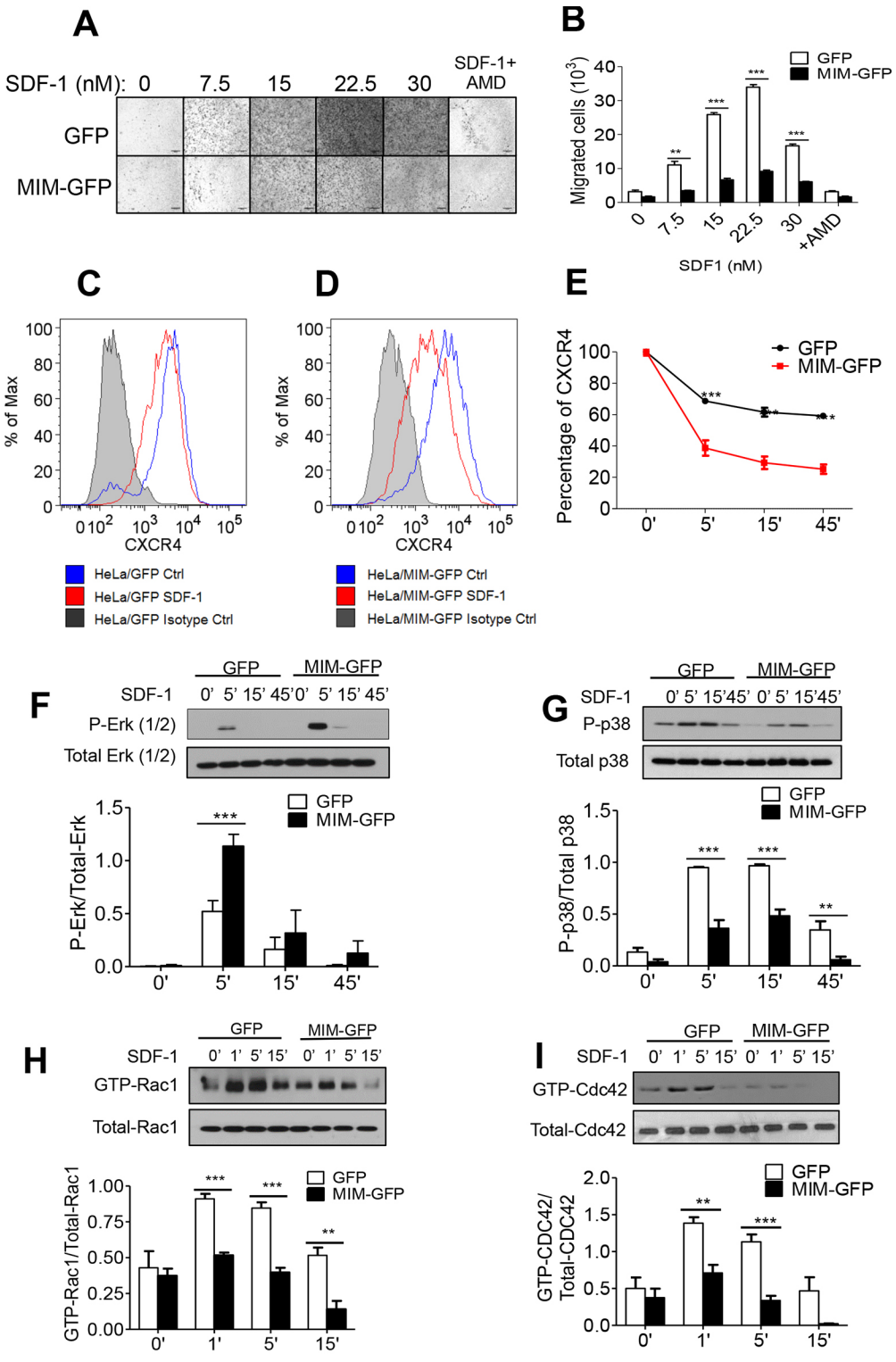

Fig. 1. MIM attenuates the chemotactic response to SDF-1 and promotes CXCR4 internalization. (A) HeLa cells expressing MIM–GFP or GFP were plated in the upper chamber of Transwell plates of which the lower chamber was filled with medium containing SDF-1 at concentrations as indicated. As a control, one plate was filled with medium supplemented with 15 nM SDF-1 plus 2 µM AMD3100 (SDF-1+AMD). After 16 h of incubation, migrated cells were stained with Crystal Violet, inspected, photographed and counted under a 20× objective lens. Scale bars: 500 µm. (B) Quantification of cell migration was based on three independent experiments as described in A. (C,D) Cells expressing GFP or MIM–GFP were treated with 100 nM SDF-1 for 15 min and subjected to flow cytometric analysis after staining with PE-conjugated monoclonal antibody directed against CXCR4. As a negative control, cells were also stained with PE–IgG antibody (isotype ctrl). Ctrl, no SDF-1. (E) The percentage of CXCR4 remaining on the cell surface after SDF-1 stimulation was calculated based on normalization to that of cells without SDF-1 treatment. (F–I) HeLa cells expressing MIM–GFP or GFP were treated with 100 nM SDF-1 for the times (min) indicated and then analyzed by western blotting for the presence of phosphorylated Erk1/2 (F, P-Erk1/2), phosphorylated p38 (G, P-p38), GTP-Rac1 (H) and GTP-Cdc42 (I). Images shown are representative of three independent experiments. All the data shown represent the mean±s.e.m. (n=3). $^{**}P$<0.01 and $^{***}P$<0.001 (Student's t-test).

fivefold increase in the number of late endosomes or MVBs, as labeled for CD63 (Fig. 5A). In contrast, no increased labeling with either a marker (EEA1) for early endosomes (Fig. S1D) or a marker (LAMP2) for lysosomes (Fig. S2A) in MIM–GFP cells was observed under the same condition, indicating that MIM promoted specifically MVB formation. Analysis of individual MIM–GFP cells revealed that about 50% of CD63 (Fig. 5B) and 45% of CD9 (Fig. S2B), both markers of MVBs, colocalized with MIM–GFP after 30 min of SDF-1 treatment. By the same time, over 60% of Myc–CXCR4 was found to colocalize with MVBs (Fig. 5C). Since there is no evidence that SDF-1 increases the expression of exogenous proteins under a constitutive promoter, the increased colocalization indicates the recruitment of MIM and CXCR4 proteins to MVBs. The MIM-promoted MVB labeling was apparently transient as it started at approximately 5 min, peaked at 30 min and gradually declined by 90 min after treatment with

Journal of Cell Science (2017) 130, 1475-1485 doi:10.1242/jcs.198937

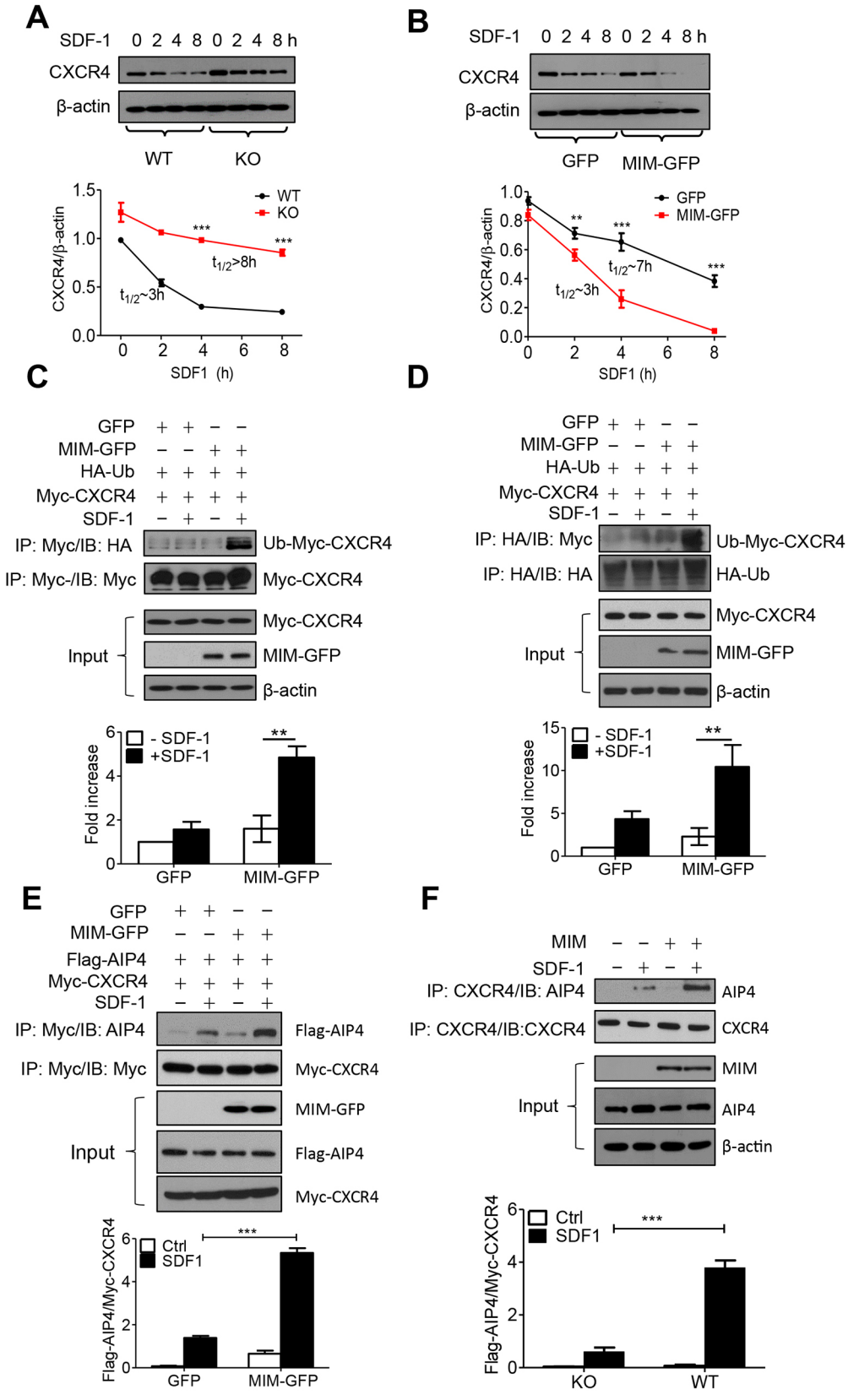

Fig. 2. MIM promotes CXCR4 degradation through AIP4-mediated ubiquitylation. (A) Cells derived from the bone marrow of either WT or MIM KO mice were pretreated with 500 µg/ml cycloheximide, followed by exposure to 100 nM SDF-1 for the times as indicated. The protein level of CXCR4 within treated cells was estimated by western blotting. (B) Cells co-expressing Myc–CXCR4, and MIM–GFP or GFP were treated with cycloheximide and SDF-1 as above. The amount of Myc–CXCR4 in treated cells was estimated by western blotting. (C,D) Cells expressing MIM–GFP or GFP were co-transfected with HA–ubiquitin and Myc–CXCR4 plasmids. The transient transfectants were lysed, and cell lysates were analyzed for Myc–CXCR4 ubiquitylation by IP with antibody against Myc antibody followed by western blotting for HA (C) and vice versa (D). (E) Cells expressing MIM–GFP or GFP were transfected with Flag–AIP4 and Myc–CXCR4 plasmids. The transient transfectants were stimulated with 100 nM SDF-1 for 30 min, lysed and subsequently subjected to IP with antibody against Myc followed by western blotting for AIP4. (F) Bone marrow cells from MIM KO or WT mice were treated with SDF-1 and subjected to IP with antibody against CXCR4, followed by western blotting for AIP4. Images shown are representative of three independent experiments. All the data shown represent the mean±s.e.m. (n=3). $^{**}P$<0.01 and $^{***}P$<0.001 (Student's t-test). IB, immunoblot; Ub, ubiquitin.

SDF-1 (Fig. S3A-C). Such temporal regulation coincided with transient colocalization of MIM–GFP with MVBs (Fig. S3D). We also observed maximal colocalization of MIM–GFP and Myc–CXCR4 at 30 min after application of SDF-1, and colocalization of these two proteins remained significant even at 90 min (Fig. S3E), which is consistent with the observed 3 h half-life of the CXCR4–GFP protein within cells (Fig. 2B), suggesting that they might interact with each other in other types of vesicle as well as in MVBs.

Journal of Cell Science (2017) 130, 1475-1485 doi:10.1242/jcs.198937

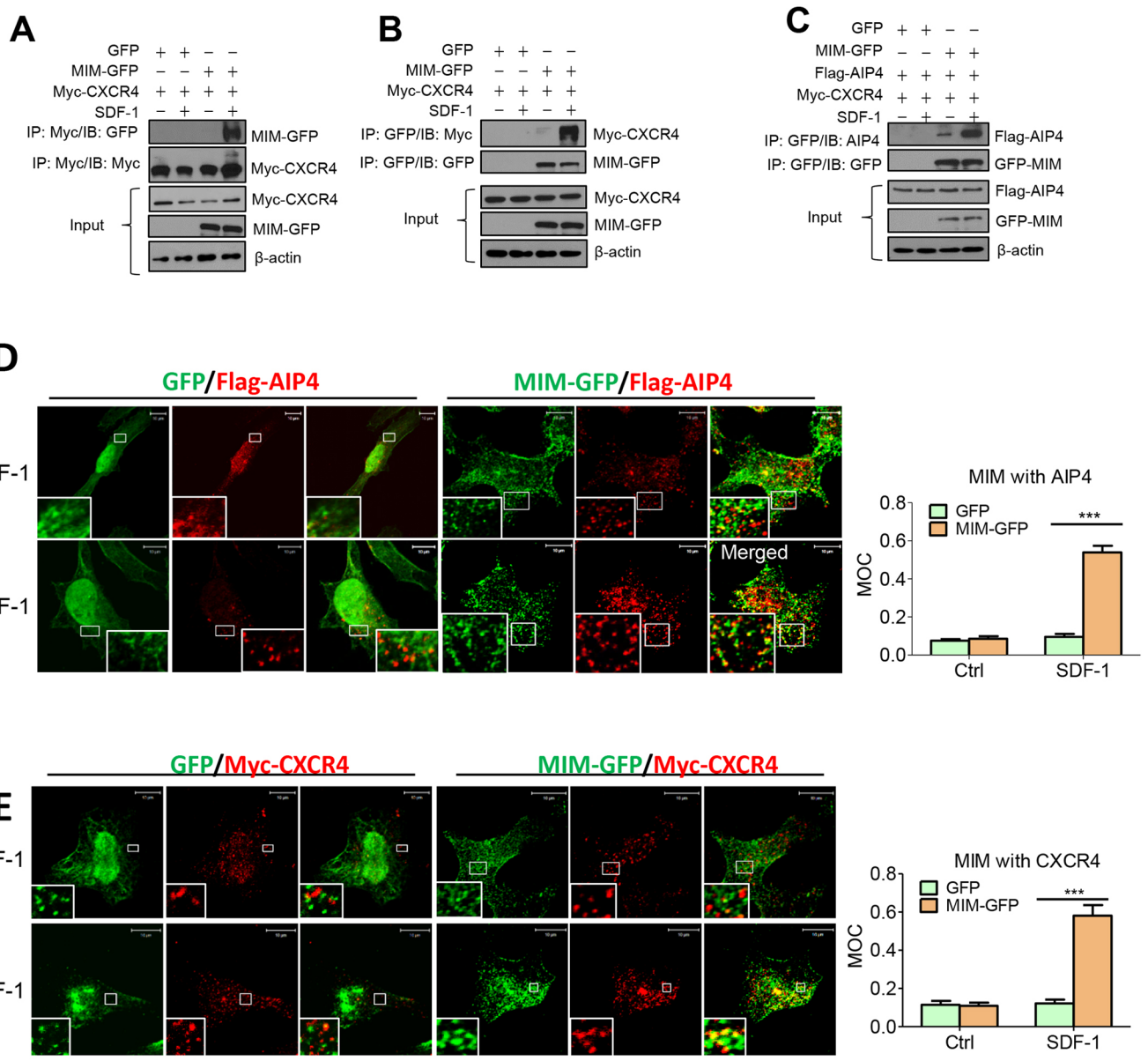

Fig. 3. MIM forms a complex with CXCR4 and AIP4. (A,B) MIM–GFP and GFP cells were transfected with Myc–CXCR4 plasmid and stimulated with 100 nM SDF-1 for 30 min. The lysates of treated cells were analyzed by IP with antibody against Myc followed by western blotting for GFP (A) or vice versa (B). (C) MIM–GFP and GFP cells were transfected with Myc–CXCR4 and Flag–AIP4 plasmids. The interaction between MIM–GFP and Flag–AIP4 was analyzed by IP using antibodies as indicated. (D) MIM–GFP or GFP cells were transfected with Flag–AIP4 and stimulated with 100 nM SDF-1 for 30 min. The treated cells were co-stained with antibodies against GFP (green) and Flag (red) and inspected by confocal microscopy. The proportion of Flag–AIP4 that colocalized with GFP or MIM–GFP was estimated by calculating MOC using ImageJ software, as described in the Materials and Methods. (E) Cells co-expressing MIM–GFP and Myc–CXCR4, or GFP and Myc–CXCR4 were stimulated with SDF-1, stained for GFP (green) and Myc (red), and the proportion of Myc–CXCR4 that colocalized with GFP or GFP-MIM quantified as described in D. All boxed areas within cells represent the zoomed area shown in the insets. Images shown are representative of three independent experiments. All the data shown represent the mean±s.e.m. (n=3). **P<0.01 and ***P<0.001 (Student's t-test). IB, immunoblot.

MIM transiently forms a complex with Rab5 and Rab7 at different times after treatment with SDF-1

In the effort to characterize further the role of MIM in intracellular trafficking, we found that binding to AIP4 was not necessary for the recruitment of MIM to MVBs because MIMΔPRD–GFP still effectively colocalized with MVBs upon treatment with SDF-1 (Fig. S4G and E), suggesting that another domain is responsible for MIM recruitment to MVBs. As endosome maturation is regulated by small GTPase Rabs, particularly by Rab5 for early endosomes and Rab7 for late endosomes (here Rab5a and Rab7a specifically have been analyzed) (Stenmark, 2009), we examined the interaction of MIM–GFP with Rab5 and Rab7 at different times after application of SDF-1. IP with an antibody against MIM readily precipitated Rab5 at 5 min (Fig. 6A) and Rab7 at 30 min (Fig. 6A). Interestingly, the interaction with both Rabs was transient. Co-precipitation of MIM–GFP with Rab7 was diminished at 90 min, the kinetics of which agree well with that for the recruitment of MIM to MVBs (Fig. S3D). Interaction of MIM–GFP with Rab7 was also confirmed by using an antibody against Rab7 in the IP step (Fig. 6B). However, the same antibody was unable to precipitate CXCR4 or AIP4 under the same condition (data not shown), suggesting that MIM interacts with Rab7

Journal of Cell Science (2017) 130, 1475-1485 doi:10.1242/jcs.198937

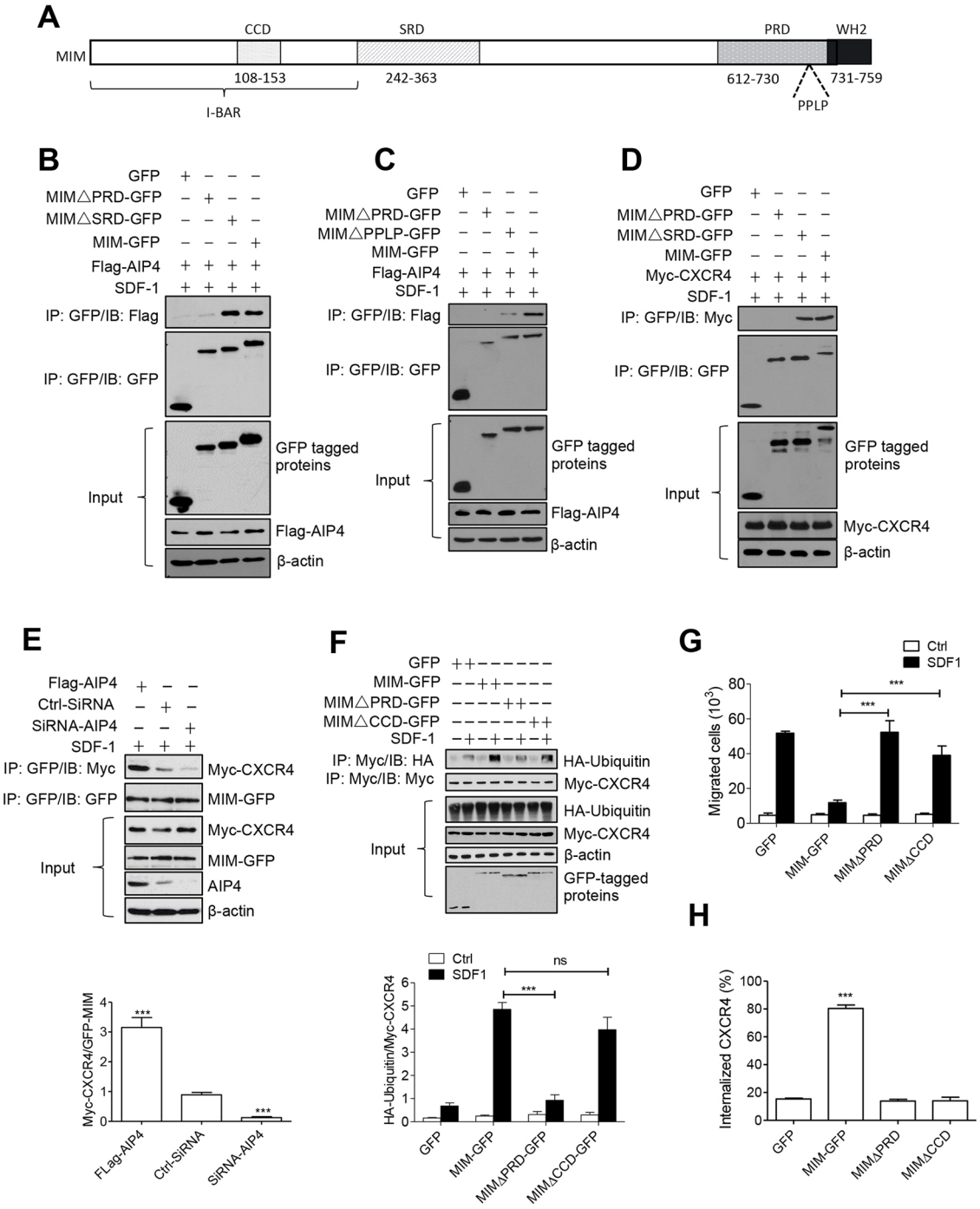

Fig. 4. Analysis of the effects of MIM variants on the response to SDF-1. (A) Schematic presentation of mouse MIM protein. CCD, coiled-coil domain; I-BAR, inverse BAR domain; SRD, serine-rich domain; PRD, proline-rich domain; and WH2, WASP homology 2 domain. (B-D) Cells expressing different combinations of MIM, AIP4 and CXCR4 proteins were treated with SDF-1 for 30 min, and then subjected to IP using antibodies as indicated for detection of the interaction between MIM variants and AIP4 (B and C) or Myc–CXCR4 (D). (E) Cells co-expressing MIM–GFP and Myc–CXCR4 were treated with either siRNA against AIP4 (SiRNA-AIP4) or control siRNA (Ctrl-SiRNA) and were further treated with 100 nM SDF-1 for 30 min. The interaction between MIM–GFP and Myc–CXCR4 in the treated cells was analyzed by co-immunoprecipitation. As a positive control, cells co-expressing MIM–GFP, Myc–CXCR4 and Flag–AIP4 were also analyzed in parallel. The data represent mean±s.e.m. (n=3). ***P<0.001 (Student's t-test). (F) Cells co-expressing HA–ubiquitin, Myc–CXCR4, and GFP or different MIM–GFP variants were stimulated with 100 nM SDF-1 for 30 min. Ubiquitylated Myc–CXCR4 proteins were analyzed by co-immunoprecipitation as indicated. (G) Cells expressing different MIM–GFP variants were analyzed for their chemotactic response to 100 nM SDF-1 as described in the legend of Fig. 1A. (H) Cells co-expressing Myc–CXCR4 with GFP or MIM–GFP variants were treated with 100 nM SDF-1 for 15 min. The surface amount of Myc–CXCR4 was estimated using flow cytometry. All the data represent mean±s.e.m. (n=3). **P<0.01 and *** P<0.001; ns, not significant (Student's t-test). IB, immunoblot.

independently of CXCR4, although we could not rule out the possibility that MIM interacts indirectly with Rab7. To determine whether endogenous MIM also interacts with Rab7, we analyzed murine Raw 264 cells, which abundantly express MIM (Fig. S1E). As shown in Fig. 6C, endogenous MIM bound effectively to both endogenous Rab7 and CXCR4 at 30 min after application of SDF-1.

Journal of Cell Science (2017) 130, 1475-1485 doi:10.1242/jcs.198937

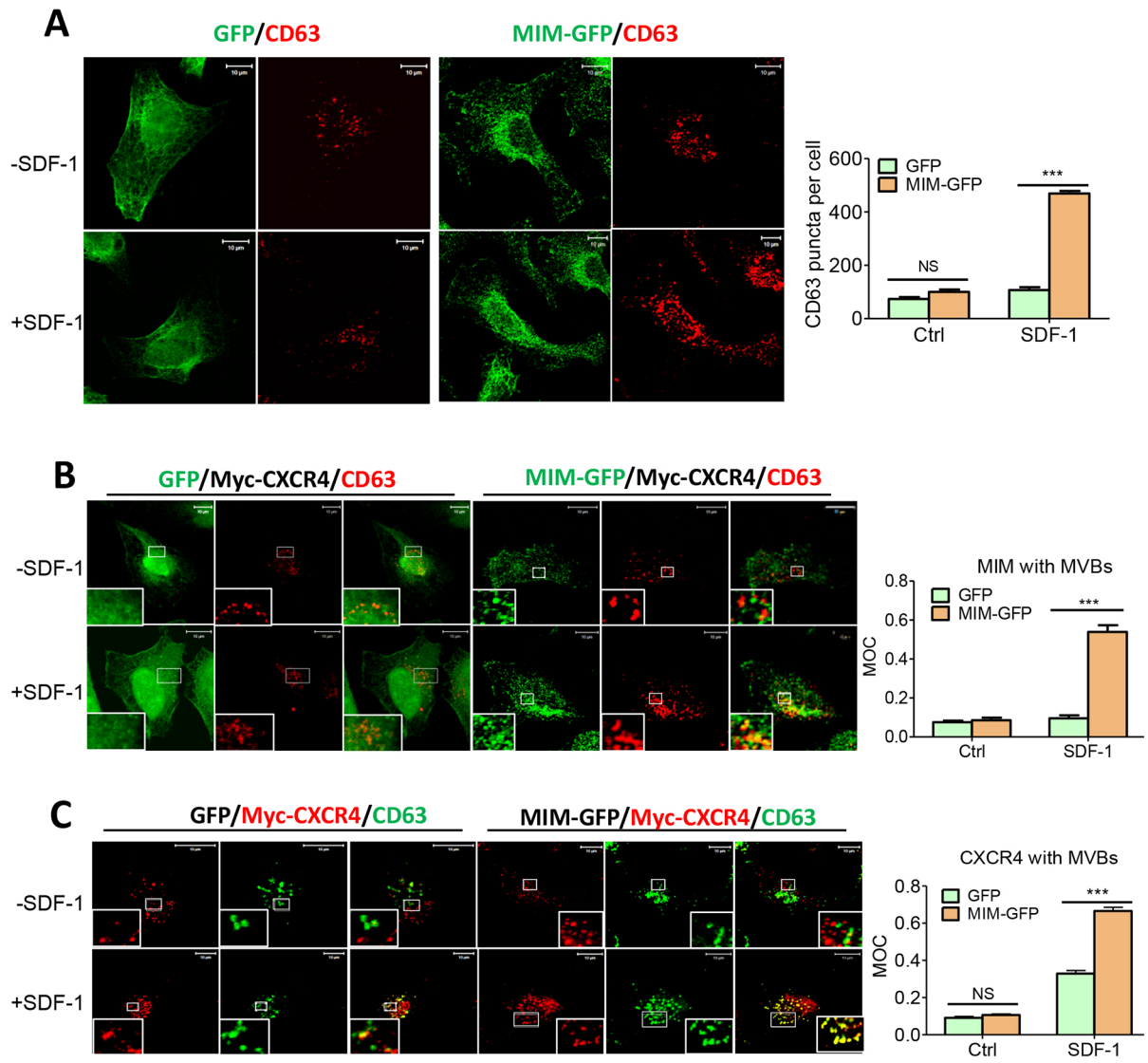

Fig. 5. MIM promotes MVB formation and sorting of CXCR4 into MVBs. (A) Cells co-expressing Flag–AIP4 with MIM–GFP or GFP were stimulated with 100 nM SDF-1 for 30 min, co-stained for GFP (green) and Flag (red) using antibodies. (B,C) Cells co-expressing Myc–CXCR4 with MIM–GFP or GFP were treated with and without SDF-1 for 30 min, stained for GFP (green) and CD63 (blue) with antibodies (B), or for Myc (red) and CD63 (green) with antibodies (C). All the stained cells were analyzed by confocal microscopy. Quantification of the proportion of red staining that colocalized with green staining was estimated based on the MOC. All the data represent mean±s.e.m. of three independent experiments in which 50 cells were examined in each experiment. ***P<0.001; NS, not significant (Student's t-test). All boxed areas within cells represent the zoomed area shown in the insets. Ctrl, no SDF-1.

Binding to Rab7 is required for MIM-mediated CXCR4 internalization

To analyze the structural basis for MIM to interact with Rab7, we analyzed a mutant containing the I-BAR domain only (MIM-I-BAR–GFP) and found that the mutant bound to Rab7 as effectively as full-length MIM–GFP (Fig. 6E), implying that the motif required to form the complex with Rab7 lies within the I-BAR domain. To determine further the sequence necessary for Rab7 binding, we analyzed a mutant that had deletion of a coiled-coil domain (CCD), which corresponds to the sequence from amino acid 108 to 153. Unlike the mutant MIMΔPRD, which retained the ability to co-precipitate with Rab7 (Fig. 6D), the mutant MIMΔCCD was unable to co-precipitate with Rab7 in response to SDF-1 (Fig. 6D), indicating that MIM interacts with AIP4 and Rab7 independently. To analyze the impact of the mutation at the CCD on the activity of MIM, we analyzed the response of cells expressing MIMΔCCD–GFP to SDF-1 and found that the mutant failed to inhibit SDF-1-mediated chemotaxis (Fig. 4G), to promote CXCR4 internalization (Fig. 4H) and to colocalize with MVBs (Fig. S4C and E). It is possible that the observed defect with MIMΔCCD–GFP might be a result of improper protein folding. Because the CCD was within the I-BAR domain, which is critical for MIM to form a dimer (Cao et al., 2012), we analyzed the dimerization of the mutant and found that it retained the same ability as the WT protein to form a homo-dimer within cells (Fig. S1F). However, we could not rule out the possibility that the mutation might impair other unrecognized functions associated with the I-BAR domain. We also analyzed the cells expressing the mutant MIM-I-BAR–GFP, which bound to Rab7 (Fig. 6E) and was recruited to MVBs upon SDF-1 application (Fig. S4D,E). Yet, the mutant was unable to promote CXCR4 internalization (Fig. 6F), indicating a necessity for the coordination between the activity for binding to Rab7 and that for binding to AIP4 in MIM-mediated regulation of CXCR4 internalization.

Journal of Cell Science (2017) 130, 1475-1485 doi:10.1242/jcs.198937

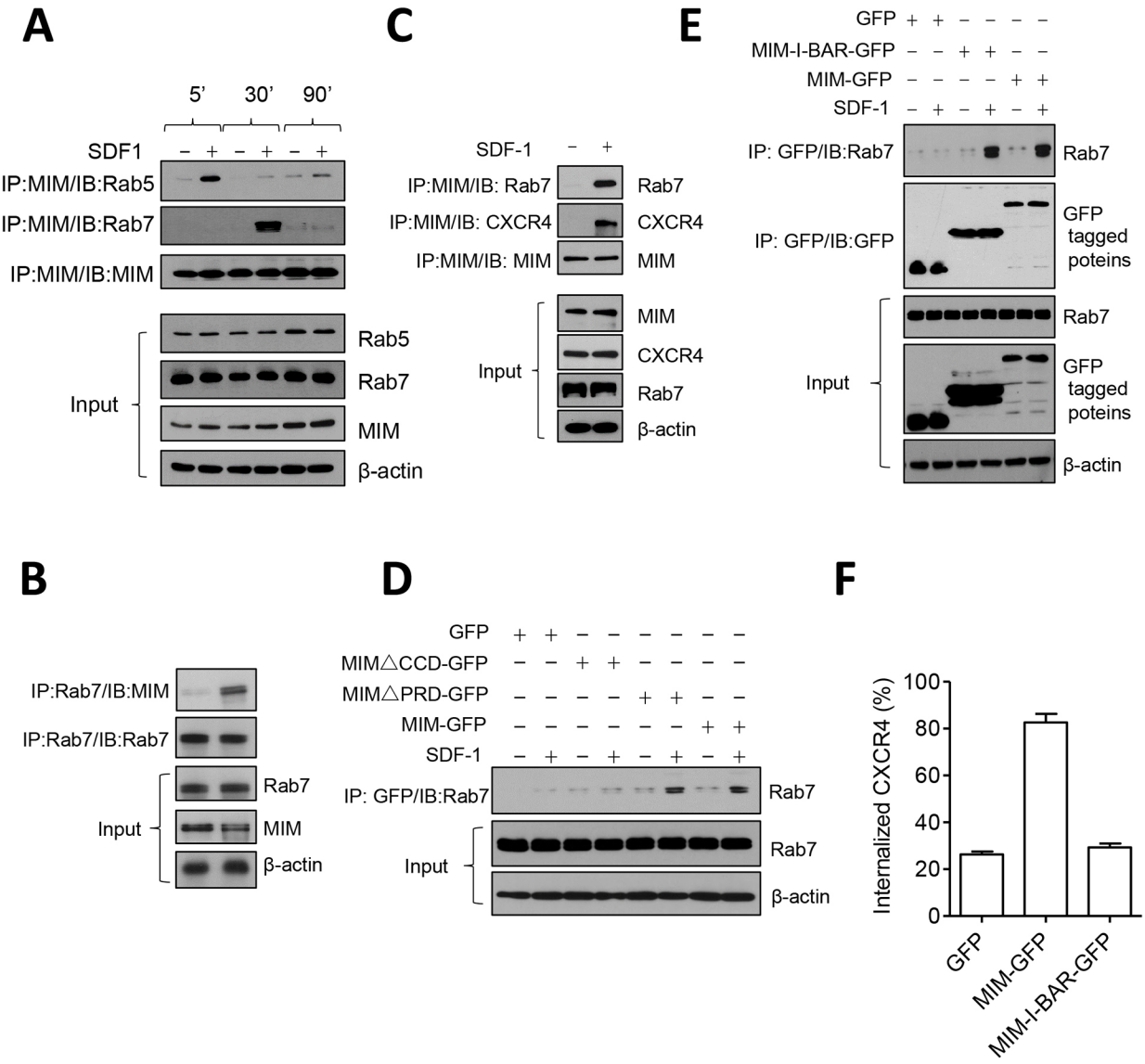

Fig. 6. MIM binds to Rab5 and Rab7 in response to SDF-1. (A) Cells expressing MIM–GFP were stimulated with 100 nM SDF-1 for 5, 30 and 90 min. The stimulated cells were lysed, and proteins were precipitated with antibody against MIM. The precipitates were than blotted for Rab5 and Rab7 using antibodies. (B) Cells expressing MIM–GFP were treated with 100 nM SDF-1 for 30 min. The lysates of treated cells were incubated with antibody against Rab7, and the precipitates were blotted for MIM using an antibody. (C) The interaction between endogenous MIM and Rab7 was analyzed by co-immunoprecipitation in Raw264 cells under conditions with and without treatment with 100 nM SDF-1 for 30 min. (D,E) Cells expressing different MIM variants were stimulated with 100 nM SDF-1 for 30 min. Interaction between MIM variants and Rab7 in the treated cells was analyzed by co-immunoprecipitation with antibodies as indicated. (F) Cells expressing GFP, or MIM–GFP or MIM-I-BAR–GFP were treated with SDF-1 for 15 min. CXCR4 internalization was estimated by flow cytometry. The data represent mean±s.e.m. (*n*=3). IB, immunoblot.

DISCUSSION

Receptor-mediated endocytosis involves the formation of clathrin-coated vesicles and the maturation of early endosomes into late endosomes or MVBs, which are defined as endocytic organelles with many intraluminal vesicles. During the formation of clathrin-coated pits, the initial generation of membrane invaginations is driven by several BAR proteins such as FCHo, FBP17, amphiphysin and endophilin, which are able to generate membranes with positive curvatures (Daumke et al., 2014). In contrast, the role of I-BAR proteins, which generate negative membrane curvatures, during the maturation of those endocytic vesicles has not yet been well illustrated. Here, we provide evidence that enforced MIM expression promotes CXCR4 internalization by promoting CXCR4 ubiquitylation via the E3 ligase AIP4 and by acting as an effector of Rab5 and Rab7, which direct the maturation of endocytic vesicles from early endosomes to late endosomes, respectively. Strikingly, MIM interacts with Rab5 transiently only during an early response and to Rab7 during a later response, implying that MIM may have a function in multiple dynamic events during endocytic processes. Although the nature of these events is currently unclear, we have observed that MIM-overexpressing cells tend to develop more MVBs in response to SDF-1 compared with control cells and that MIM-promoted MVB formation coincides with the binding of MIM to Rab7, and both occurred of these events peaked at approximately 30 min after stimulation with SDF-1. In this regard, it is interesting to know that biogenesis of intraluminal vesicles requires the generation of membranes with negative curvature, which are thought to be sculpted to a sufficient degree

Journal of Cell Science (2017) 130, 1475-1485 doi:10.1242/jcs.198937

by ESCRT-III helixes following sorting of ubiquitylated cargos onto the limiting membrane under the concerted action of ESCRT-0, -I and -II (Henne et al., 2013; Olmos and Carlton, 2016). Yet, the detailed mechanism for the initiation of negatively curved membranes and the functional relationship between Rab7 signaling and ESCRTs remains elusive. As MIM generates negatively curved membrane and promotes receptor ubiquitylation – the event that leads to association with the ESCRT complexes (Raiborg and Stenmark, 2009) – the interactions of MIM, Rabs and AIP4 could represent a new mechanism by which Rabs direct negative curvature that is used for membrane deformation, such as in the fission process mediated by the ESCRT complex. One possibility is that Rab GTPases determine where MIM is to act and that MIM-mediated activation of AIP4 directs which cargos are to be sorted into endocytic vesicles. Consistent with this view, there are several recent reports that Ivy1p, which is a yeast protein possessing an I-BAR-like domain that is otherwise unrelated to MIM that also acts as an effector of Ypt7 (yeast ortholog of Rab7), is implicated in endocytic sorting, vacuole morphology and membrane homeostasis (Itoh et al., 2016; Numrich et al., 2015). In agreement with our findings, overexpression of Ivy1p can cause dramatic accumulation of MVBs in yeast, and there is evidence for the association of Ivy1p protein with vacuole membrane domains with negative curvature (Numrich et al., 2015). Hence, our data together with other studies demonstrate that MIM is implicated in the membrane dynamics of endocytic vesicles. In addition to its association with endosomes, MIM has been also implicated in antagonizing the complex of cortactin and the CD2-associated protein, and in inhibition of the endocytosis of EGF and in directional border cell migration in *Drosophila* (Quinones et al., 2010). The difference between our observations and that report may reflect the multiple roles of MIM in endocytosis under different contexts, as described in these studies.

Another striking observation that we made here is that MIM binds to Rab7 and AIP4 only upon stimulation with SDF-1, indicating that there may be an activation step with MIM that takes place during the response to the chemokine. While the nature of MIM activation is unknown, IRSp53, a MIM-related molecule, has a closed inactive conformation resulting from an intramolecular interaction (Kast et al., 2014), which can then be activated upon binding to Cdc42 (Disanza et al., 2013). However, the mutant MIM-I-BAR, like full-length MIM, also shows SDF-1-dependent binding to Rab7. Furthermore, AIP4-mediated ubiquitylation is an early event during CXCR4 internalization (Bhandari et al., 2009). Hence, it is likely that MIM acts an effector of Rab5 and Rab7, and as a signaling factor downstream of AIP4. Further characterization of the mechanism for these interactions should unveil how MIM is regulated to control intracellular trafficking.

Aberrant expression of MIM and CXCR4 has been shown to be common in many advanced cancers. Since CXCR4 has an established role in directing stem cells to their niches and in the organotropism of metastatic tumor cells, the identified pathway for MIM-mediated regulation of CXCR4 indicates a new oncogenic process that may influence profoundly the interaction of tumors with their microenvironments. However, MIM downregulates CXCR4 through a direct interaction with AIP4 but not with CXCR4, suggesting that MIM may regulate post-translational modification of other receptors that are targeted by AIP4. Because AIP4 is a member of the family of NEDD4 E3 ligases that are involved in the pathogenesis of a wide spectrum of malignancies as either tumor suppressors or proto-oncogenes (Zou et al., 2015), the complexity of these proteins may underlie the observed complicated role of MIM in tumor progression.

MATERIALS AND METHODS

Cells and cell lines

HeLa cells were cultured in Dulbecco's modified Eagle's medium (DMEM) (Corning, NY) that had been supplemented with 10% fetal bovine serum (Hyclone, Logan, UT), 100 unit/ml penicillin and 100 µg/ml streptomycin under 5% CO_2 at 37°C. DNA transfection was performed, and stably-transfected cells were selected as described previously (Lin et al., 2005). All the cells were tested for contamination routinely every 2 months. Mononuclear cells were purified from the bone marrow of either wild-type or MIM KO mice at the age of 8 weeks, as described previously (Zhan et al., 2016).

Antibodies and reagents

Antibodies against CXCR4 (Cat. No. sc-53534) and CD63 (Cat. No. sc-15363) were purchased from Santa Cruz Biotechnology. Antibody against Flag (Cat. No. MAB3118) and Rac1 (Cat. No. 05-389) were purchased from Millipore. Antibodies against phosphorylated p38 (Cat. No. 9215s), p38 (Cat. No. 9212S), phosphorylated Erk1/2 (Cat. No.4377S), Erk1/2 (Cat. No. 9102S) and Cdc42 (Cat. No. 2462S) were purchased from Cell Signaling Technology. FITC-conjugated goat anti-rabbit (Cat. No. INV-A21311), Alexa-Fluor-568-conjugated goat anti-mouse (Cat. No. INV-A21134) and Alexa-Fluor-633-conjugated goat anti-mouse (Cat. No. INV-A21050) antibodies were purchased from Invitrogen. SDF-1 (Cat. No. 581206), and anti-HA (Cat. No. 660002) and PE-conjugated anti-human CXCR4 antibodies (Cat. No. 306506) were purchased from BioLegend. Antibodies against MIM (Cat. No. INV-PA517047) and Myc (Cat. No. INV-MA1980), and protein A/G agarose beads (Cat. No. 20423) were purchased from Thermo Scientific Pierce. Antibody against EEA1 (Cat. No. 610456) was from BD Biosciences. Monoclonal antibodies against Rab7 (Cat. No. R8779) and Rab5a (Cat. No. WH0005868M9) were purchased from Sigma-Aldrich. PBS (Cat. No. 21-040-CV) was purchased from Corning (Corning, NY). Cycloheximide (CHX, Cat. No. C4859), a mixture of siRNAs against AIP4 (Cat. No. EHU133631) targeting 18 different sites and control siRNA with a scrambled sequence were purchased from Sigma-Aldrich.

Plasmids

Plasmids encoding MIM–GFP, MIMΔPRD, MIMΔCCD and MIMΔSRD were prepared as described previously (Wang et al., 2007). Flag–ITCH (AIP4) plasmid, which encodes AIP4 tagged with three Flag epitopes and is based on pCMV2-FLAG vector, was purchased from Sino Biological Company (North Wales, PA; Cat. No. HG11131-M-F). Myc–DDK-CXCR4 plasmid was purchased from OriGene (Cat. No. RC202069). HA–ubiquitin plasmid was purchased from Addgene (Cat. No. 18712).

Immunoblot analysis

Immunoblot assay was performed as described previously (Yu et al., 2011). Briefly, cells were lysed with RIPA lysis buffer supplemented with anti-protease tablet (Roche) and anti-phosphatase cocktails (Sigma-Aldrich). Cell lysates were prepared by centrifuging followed by boiling with sample buffer (Thermo Fisher Scientific). Aliquots of the lysates were loaded into gels for SDS-PAGE followed by transfer to a PVDF membrane. The membrane was blocked with 5% milk TBST solution (10 mM Tris-HCl, pH 8.0, 150 mM NaCl and 0.1% Tween 20) at room temperature for 1 h, incubated with primary antibody (all used at 1 µg/ml) overnight at 4°C with agitation, rinsed with TBST and then incubated with horseradish peroxidase (HRP)-conjugated secondary antibody at room temperature for 2 h. After washing three times with TBST, enhanced chemiluminescence detection solution (PIERCE, Rockford, IL) was applied to the membrane. The proteins probed were visualized by using X-autoradiography. Densitometry analysis was performed with gel images from three independent experiments using ImageJ software.

Cell migration assay

Serum-free DMEM was added to the lower chamber of a Transwell plate with an insert of pore size of 8 µm (Corning). After incubation overnight in a cell culture incubator, cells in serum-free DMEM were plated at 2×10^5/well on the upper chamber of the plate, and 750 µl DMEM containing 15 nM

SDF-1 was added to the lower chamber. For the control sample, 2 µM AMD3100 (Sigma), a specific inhibitor of CXCR4, was added to the lower chamber 30 min before adding SDF-1. After incubation at 37°C for 16 h, the cells on the insert were washed with PBS twice and fixed with 4% paraformaldehyde for 5 min followed by washing twice with PBS. To count cells, 200 µl methanol was added to the plate and incubated at room temperature for 20 min, followed by staining of cells with 0.1% Crystal Violet for 15 min. After washing with PBS, non-migrated cells on the upper surface of the insert were carefully scraped with cotton swabs. Migrated cells were inspected microscopically at 20× magnification, and the cells within nine microscopic fields were counted for each plate.

Flow cytometry analysis

HeLa cells overexpressing GFP or MIM–GFP and grown in a 10-cm dish were treated with 1 ml of 0.2% EDTA Cell Dissociation Reagent (Thermo Fisher Scientific). The detached cells were incubated with 2 ml DMEM, transferred into a fresh 10-ml tube containing 5 ml DMEM and 100 nM SDF-1. After incubation for different time periods, cells were immediately placed on ice, followed by addition of 2 ml of pre-chilled PBS containing 0.75% BSA and 5 mM EDTA (FACS buffer). The treated cells were centrifuged at 112 ***g*** for 3 min at 4°C, and the cell pellet was stained with PE-conjugated anti-human-CXCR4 antibody (1 µg/ml) and incubated at 4°C for 1 h in a covered box. As the control, cells were treated with PE-conjugated anti-IgG antibody in parallel. After staining, 500 µl FACS buffer was added to the cells followed by centrifugation. The supernatant was removed by aspiration, and the pelleted cells were washed with PBS three times, fixed with 4% paraformaldehyde and then subjected to flow cytometry analysis with a BD LSRFortessa flow cytometry system. The data were analyzed by using FlowJo software version 8.8.7.

Immunofluorescence microscopy

Sterilized glass coverslips were placed in a 6-well plate and incubated with 5 µg/ml fibronectin (Life Technology) for 30 min at room temperature. 2×10^5 cells were plated into each well and cultured in DMEM supplemented with 10% FBS and 1% penicillin-streptomycin overnight. Cells were then transfected with plasmids by using FuGene Transfection Reagent (Active Motif, Carlsbad, CA) according to the manufacturer's instructions. After 16 h, cells were cultured in DMEM supplemented with 10% FBS for 24 h, and the medium was replaced with DMEM and incubated for 2 h. The starved cells were incubated with 100 nM SDF-1 (or vehicle as control) for 30 min. After washing twice with PBS, cells were fixed with 4% paraformaldehyde at room temperature for 10 min, and permeabilized with 0.05% saponin for 10 min. The fixed cells were blocked by 200 µl PBS supplemented with 5% goat serum, incubated with 100 µl of blocking buffer with the primary antibody (all used at 5 µg/ml) for 1 h at room temperature. After rinsing three times with PBS, the cells were incubated with Alexa-Flour-conjugated secondary antibody for 1 h, and mounted on a glass slide with 20 µl of Mounting Medium (Kirkegaard & Perry Laboratories, MD). The slide was sealed with nail polish, and the stained cells were inspected using a Zeiss LSM 510 laser scanning confocal imaging system using a Plan-Apo 63×/1.4 numerical aperture oil lens. The digital images were captured using an acquisition setting that was applied to all the samples analyzed in parallel. In each group, all the images were taken and presented at the same settings for brightness and contrasts. Protein colocalization was quantified based on MOC (Dunn et al., 2011), which was calculated by using an ImageJ plugin. The value of MOC ranges from 0 to 1, and represents the proportion of red fluorescence intensity that is in the green channel. As a negative control, one of a pair of images captured under the red channel was rotated by 90° and then imposed onto the green image. The resulting MOC was considered as the background and subtracted from the MOC calculated from the original images (Fig. S4J). Quantification of stained puncta was conducted by using the ImageJ software.

Protein degradation assay

Bone marrow cells or HeLa cells expressing Myc–CXCR4 or MIM–GFP were plated at a density of 8×10^5/well in a 6-well plate. After 24 h incubation, cells were treated with 0.5 mg/ml cycloheximide for 30 min at 37°C and incubated with 15 nM SDF-1 for the times as indicated at 37°C and under 5% CO_2. The treated cells were then placed on ice and lysed using RIPA buffer. The protein content of cell lysates was estimated with a BCA assay kit (Thermo Fisher Scientific), and lysates containing equal amounts of proteins were analyzed by 10% acrylamide SDS-PAGE. MIM–GFP and Myc–CXCR4 proteins were detected by western blotting with anti-Myc and anti-MIM antibodies (1 µg/ml), respectively. The same blots were stripped and re-blotted for β-actin as the loading control.

Ubiquitylation and co-immunoprecipitation assay

To evaluate CXCR4 ubiquitylation, cell lysates were subjected IP followed by immunoblot as described previously (Zhan et al., 2016). Briefly, cells grown in 10-cm dishes were transiently transfected with plasmids encoding 5 µg Myc–CXCR4, 5 µg MIM–GFP and 5 µg HA–ubiquitin. 24 h later, the transfection medium was replaced with DMEM plus 10% FBS. The cells were incubated for an additional 24 h, starved in DMEM for 2 h and treated with 100 nM SDF-1 for 30 min. The lysates of treated cells were incubated with 20 µl 50% protein-A beads (Invitrogen) for 90 min at 4°C and centrifuged at 100 ***g***. The supernatant was mixed with 5 µg/ml anti-Myc antibody, incubated overnight at 4°C and mixed with 100 µl of protein-A beads. After incubation for 2 h at 4°C, the mixture was centrifuged at 2000 rpm for 30 sec. The pellet was washed three times with 0.5 ml lysis buffer, dissolved in 60 µl SDS sample buffer, boiled for 10 min and subjected to SDS-PAGE followed by western blot using anti-HA antibody. In a parallel experiment, anti-HA antibody was used in IP and the anti-Myc antibody was used in western blot to verify the co-precipitation.

Acknowledgements

We thank Drs. Yanbao Xiong and Tailan Zhan for assistance with flow cytometry and immunofluorescence analyses. We also thank the Confocal Microscopy Core at University of Maryland School of Medicine Center for Innovative Biomedical Resources for help in confocal microscopy analyses.

Competing interests

The authors declare no competing or financial interests.

Author contributions

L.L. and S.S.B. performed the work described. L.L. and X.Z. designed experiments and wrote the manuscript. N.G. and M.J. are the supervisors of L.L. in China and contributed to discussions and manuscript preparation.

Funding

This research was supported by the National Cancer Institute (R01 CA113809 to X.Z.); National Natural Science Foundation of China for Key Project of International Cooperation (61420106012, to N.G.); National High-Tech Research and Development Project (863 Project from the Ministry of Science and Technology of the People's Republic of China, 2013AA032205 to M.J.); and the Maryland Stem Cell Research Fund (2012-0081 to X.Z.). Deposited in PMC for release after 12 months.

Supplementary information

Supplementary information available online at
http://jcs.biologists.org/lookup/doi/10.1242/jcs.198937.supplemental

References

Agarwal, E., Robb, C. M., Smith, L. M., Brattain, M. G., Wang, J., Black, J. D. Chowdhury, S. (2017). Role of Akt2 in regulation of metastasis suppressor 1 expression and colorectal cancer metastasis. *Oncogene*. [Epub ahead of print] doi: 10.1038/onc.2016.460

Bedford, M. T., Chan, D. C. and Leder, P. (1997). FBP WW domains and the Abl SH3 domain bind to a specific class of proline-rich ligands. *EMBO J.* **16**, 2376-2383.

Bhandari, D., Robia, S. L. and Marchese, A. (2009). The E3 ubiquitin ligase atrophin interacting protein 4 binds directly to the chemokine receptor CXCR4 via a novel WW domain-mediated interaction. *Mol. Biol. Cell* **20**, 1324-1339.

Cao, M., Zhan, T., Ji, M. and Zhan, X. (2012). Dimerization is necessary for MIM-mediated membrane deformation and endocytosis. *Biochem. J.* **446**, 469-475.

Chen, H. I. and Sudol, M. (1995). The WW domain of Yes-associated protein binds a proline-rich ligand that differs from the consensus established for Src homology 3-binding modules. *Proc. Natl. Acad. Sci. USA* **92**, 7819-7823.

Daumke, O., Roux, A. and Haucke, V. (2014). BAR domain scaffolds in dynamin-mediated membrane fission. *Cell* **156**, 882-892.

Dawson, J. C., Legg, J. A. and Machesky, L. M. (2006). Bar domain proteins: a role in tubulation, scission and actin assembly in clathrin-mediated endocytosis. *Trends Cell Biol.* **16**, 493-498.

Disanza, A., Bisi, S., Winterhoff, M., Milanesi, F., Ushakov, D. S., Kast, D., Marighetti, P., Romet-Lemonne, G., Müller, H.-M., Nickel, W. et al. (2013). CDC42 switches IRSp53 from inhibition of actin growth to elongation by clustering of VASP. *EMBO J.* **32**, 2735-2750.

Dunn, K. W., Kamocka, M. M. and McDonald, J. H. (2011). A practical guide to evaluating colocalization in biological microscopy. *Am. J. Physiol. Cell Physiol.* **300**, C723-C742.

Guerra, F. and Bucci, C. (2016). Multiple roles of the small GTPase Rab7. *Cells* **5**, 35.

Henne, W. M., Stenmark, H. and Emr, S. D. (2013). Molecular mechanisms of the membrane sculpting ESCRT pathway. *Cold Spring Harb. Perspect. Biol.* **5**, a016766

Itoh, Y., Kida, K., Hanawa-Suetsugu, K. and Suetsugu, S. (2016). Yeast Ivy1p is a putative I-BAR-domain protein with pH-sensitive filament forming ability in vitro. *Cell Struct. Funct.* **41**, 1-11.

Kast, D. J., Yang, C., Disanza, A., Boczkowska, M., Madasu, Y., Scita, G., Svitkina, T. and Dominguez, R. (2014). Mechanism of IRSp53 inhibition and combinatorial activation by Cdc42 and downstream effectors. *Nat. Struct. Mol. Biol.* **21**, 413-422.

Lee, Y.-G., Macoska, J. A., Korenchuk, S. and Pienta, K. J. (2002). MIM, a potential metastasis suppressor gene in bladder cancer. *Neoplasia* **4**, 291-294.

Lee, S. H., Kerff, F., Chereau, D., Ferron, F., Klug, A. and Dominguez, R. (2007). Structural basis for the actin-binding function of missing-in-metastasis. *Structure* **15**, 145-155.

Lin, J., Liu, J., Wang, Y., Zhu, J., Zhou, K., Smith, N. and Zhan, X. (2005). Differential regulation of cortactin and N-WASP-mediated actin polymerization by missing in metastasis (MIM) protein. *Oncogene* **24**, 2059-2066.

Liu, K., Wang, G., Ding, H., Chen, Y., Yu, G. and Wang, J. (2010). Downregulation of metastasis suppressor 1(MTSS1) is associated with nodal metastasis and poor outcome in Chinese patients with gastric cancer. *BMC Cancer* **10**, 428.

Lu, P. J., Zhou, X. Z., Shen, M. and Lu, K. P. (1999). Function of WW domains as phosphoserine- or phosphothreonine-binding modules. *Science* **283**, 1325-1328.

Marchese, A. (2009). Ubiquitination of chemokine receptors. *Methods Enzymol.* **460**, 413-422.

Marchese, A. (2014). Endocytic trafficking of chemokine receptors. *Curr. Opin. Cell Biol.* **27**, 72-77.

Marchese, A. and Benovic, J. L. (2001). Agonist-promoted ubiquitination of the G protein-coupled receptor CXCR4 mediates lysosomal sorting. *J. Biol. Chem.* **276**, 45509-45512.

Marchese, A., Raiborg, C., Santini, F., Keen, J. H., Stenmark, H. and Benovic, J. L. (2003). The E3 ubiquitin ligase AIP4 mediates ubiquitination and sorting of the G protein-coupled receptor CXCR4. *Dev. Cell* **5**, 709-722.

McCormick, P. J., Segarra, M., Gasperini, P., Gulino, A. V. and Tosato, G. (2009). Impaired recruitment of Grk6 and beta-Arrestin 2 causes delayed internalization and desensitization of a WHIM syndrome-associated CXCR4 mutant receptor. *PLoS ONE* **4**, e8102.

Mertz, K. D., Pathria, G., Wagner, C., Saarikangas, J., Sboner, A., Romanov, J., Gschaider, M., Lenz, F., Neumann, F., Schreiner, W. et al. (2014). MTSS1 is a metastasis driver in a subset of human melanomas. *Nat. Commun.* **5**, 3465.

Mizuno-Yamasaki, E., Rivera-Molina, F. and Novick, P. (2012). GTPase networks in membrane traffic. *Annu. Rev. Biochem.* **81**, 637-659.

Nixdorf, S., Grimm, M.-O., Loberg, R., Marreiros, A., Russell, P. J., Pienta, K. J. and Jackson, P. (2004). Expression and regulation of MIM (Missing In Metastasis), a novel putative metastasis suppressor gene, and MIM-B, in bladder cancer cell lines. *Cancer Lett.* **215**, 209-220.

Numrich, J., Peli-Gulli, M.-P., Arlt, H., Sardu, A., Griffith, J., Levine, T., Engelbrecht-Vandre, S., Reggiori, F., De Virgilio, C. and Ungermann, C. (2015). The I-BAR protein Ivy1 is an effector of the Rab7 GTPase Ypt7 involved in vacuole membrane homeostasis. *J. Cell Sci.* **128**, 2278-2292.

Olmos, Y. and Carlton, J. G. (2016). The ESCRT machinery: new roles at new holes. *Curr. Opin. Cell Biol.* **38**, 1-11.

Parr, C. and Jiang, W. G. (2009). Metastasis suppressor 1 (MTSS1) demonstrates prognostic value and anti-metastatic properties in breast cancer. *Eur. J. Cancer* **45**, 1673-1683.

Quinones, G. A., Jin, J. and Oro, A. E. (2010). I-BAR protein antagonism of endocytosis mediates directional sensing during guided cell migration. *J. Cell Biol.* **189**, 353-367.

Raiborg, C. and Stenmark, H. (2009). The ESCRT machinery in endosomal sorting of ubiquitylated membrane proteins. *Nature* **458**, 445-452.

Saarikangas, J., Zhao, H., Pykäläinen, A., Laurinmäki, P., Mattila, P. K., Kinnunen, P. K. J., Butcher, S. J. and Lappalainen, P. (2009). Molecular mechanisms of membrane deformation by I-BAR domain proteins. *Curr. Biol.* **19**, 95-107.

Saarikangas, J., Mattila, P. K., Varjosalo, M., Bovellan, M., Hakanen, J., Calzada-Wack, J., Tost, M., Jennen, L., Rathkolb, B., Hans, W. et al. (2011). Missing-in-metastasis MIM/MTSS1 promotes actin assembly at intercellular junctions and is required for integrity of kidney epithelia. *J. Cell Sci.* **124**, 1245-1255.

Saarikangas, J., Kourdougli, N., Senju, Y., Chazal, G., Segerstråle, M., Minkeviciene, R., Kuurne, J., Mattila, P. K., Garrett, L., Holter, S. M. et al. (2015). MIM-induced membrane bending promotes dendritic spine initiation. *Dev. Cell* **33**, 644-659.

Schemionek, M., Herrmann, O., Reher, M. M., Chatain, N., Schubert, C., Costa, I. G., Hanzelmann, S., Gusmao, E. G., Kintsler, S., Braunschweig, T. et al. (2015a). Mtss1 is a critical epigenetically regulated tumor suppressor in CML. *Leukemia* **30**, 823-832.

Schemionek, M., Kharabi Masouleh, B., Klaile, Y., Krug, U., Hebestreit, K., Schubert, C., Dugas, M., Buchner, T., Wormann, B., Hiddemann, W. et al. (2015b). Identification of the adapter molecule MTSS1 as a potential oncogene-specific tumor suppressor in acute myeloid leukemia. *PLoS ONE* **10**, e0125783.

Spiegel, A., Kollet, O., Peled, A., Abel, L., Nagler, A., Bielorai, B., Rechavi, G., Vormoor, J. and Lapidot, T. (2004). Unique SDF-1-induced activation of human precursor-B ALL cells as a result of altered CXCR4 expression and signaling. *Blood* **103**, 2900-2907.

Stenmark, H. (2009). Rab GTPases as coordinators of vesicle traffic. *Nat. Rev. Mol. Cell Biol.* **10**, 513-525.

Wang, Y., Zhou, K., Zeng, X., Lin, J. and Zhan, X. (2007). Tyrosine phosphorylation of missing in metastasis protein is implicated in platelet-derived growth factor-mediated cell shape changes. *J. Biol. Chem.* **282**, 7624-7631.

Xia, S., Li, X., Johnson, T., Seidel, C., Wallace, D. P. and Li, R. (2010). Polycystin-dependent fluid flow sensing targets histone deacetylase 5 to prevent the development of renal cysts. *Development* **137**, 1075-1084.

Xie, F., Ye, L., Ta, M., Zhang, L. and Jiang, W. G. (2011). MTSS1: a multifunctional protein and its role in cancer invasion and metastasis. *Front. Biosci.* **3**, 621-631.

Yu, D., Zhan, X. H., Niu, S., Mikhailenko, I., Strickland, D. K., Zhu, J., Cao, M. and Zhan, X. (2011). Murine missing in metastasis (MIM) mediates cell polarity and regulates the motility response to growth factors. *PLoS ONE* **6**, e20845.

Yu, D., Zhan, X. H., Zhao, X. F., Williams, M. S., Carey, G. B., Smith, E., Scott, D., Zhu, J., Guo, Y., Cherukuri, S. et al. (2012). Mice deficient in MIM expression are predisposed to lymphomagenesis. *Oncogene* **31**, 3561-3568.

Zhan, T., Cao, C., Li, L., Gu, N., Civin, C. I. and Zhan, X. (2016). MIM regulates the trafficking of bone marrow cells via modulating surface expression of CXCR4. *Leukemia* **30**, 1327-1334.

Zimmerberg, J. and McLaughlin, S. (2004). Membrane curvature: how BAR domains bend bilayers. *Curr. Biol.* **14**, R250-R252.

Zou, X., Levy-Cohen, G. and Blank, M. (2015). Molecular functions of NEDD4 E3 ubiquitin ligases in cancer. *Biochim. Biophys. Acta* **1856**, 91-106.